



Polylysine-decorated macroporous microcarriers laden with adipose-derived stem cells promote nerve regeneration in vivo

Yi Sun^{a,c,1}, Xiaoqi Chi^{a,1}, Haoye Meng^{a,b,1}, Mengjiao Ma^a, Jing Wang^b, Zhaoxuan Feng^a, Qi Quan^b, Guodong Liu^a, Yansen Wang^a, Yajie Xie^a, Yudong Zheng^{a,*}, Jiang Peng^{b,d,**}

^a School of Materials Science and Engineering, University of Science and Technology Beijing, Beijing, 100083, PR China

^b Institute of Orthopedics, Chinese PLA General Hospital, Beijing Key Lab of Regenerative Medicine in Orthopedics, Key Lab of Musculoskeletal Trauma & War Injuries, PLA, No.28 Fuxing Road, Beijing, 100853, PR China

^c Qingdao National Laboratory for Marine Science and Technology, Qingdao, 266237, PR China

^d Co-innovation Center of Neuroregeneration, Nantong University, Nantong, Jiangsu Province, 226007, PR China

ARTICLE INFO

Keywords:

Chitosan microcarriers
Polylysine
Adipose-derived stem cells
Peripheral nerve repair
Cell transplantation

ABSTRACT

Cell transplantation is an effective strategy to improve the repair effect of nerve guide conduits (NGCs). However, problems such as low loading efficiency and cell anoikis undermine the outcomes. Microcarriers are efficient 3D cell culture scaffolds, which can also prevent cell anoikis by providing substrate for adhesion during transplantation. Here, we demonstrate for the first time microcarrier-based cell transplantation in peripheral nerve repair. We first prepared macroporous chitosan microcarriers (CSMCs) by the emulsion-phase separation method, and then decorated the CSMCs with polylysine (pl-CSMCs) to improve cell affinity. We then loaded the pl-CSMCs with adipose-derived stem cells (ADSCs) and injected them into electrospun polycaprolactone/chitosan NGCs to repair rat sciatic nerve defects. The ADSCs-laden pl-CSMCs effectively improved nerve regeneration as demonstrated by evaluation of histology, motor function recovery, electrophysiology, and gastrocnemius recovery. With efficient cell transplantation, convenient operation, and the multiple merits of ADSCs, the ADSCs-laden pl-CSMCs hold good potential in peripheral nerve repair.

1. Introduction

Peripheral nerve injury is a frequently occurred disease that can cause great trouble to the patients [1,2]. Successful repair of large nerve peripheral defects has been an on-going clinical challenge. Among the various solutions, repairing nerve defects with synthetic nerve guide conduits (NGCs) is considered as a promising strategy to replace nerve autograft, which is currently the “gold standard” for repairing large nerve defects [3,4]. Synthetic NGCs have multiple merits, such as unlimited sources, free of immunogenicity, customizable size and structure, and the potential for incorporating various functions. Therefore, much effort has been dedicated to the development of synthetic NGCs [5–10]. However, due to the lack of biological factors, satisfying recovery is seldomly achieved with synthetic NGCs alone.

Cell transplantation is an effective method to create a favorable environment for regeneration [11,12]. NGCs seeded with cells have been shown to have better recovery results [13,14]. Therefore, many studies have been dedicated to cell transplantation in nerve regeneration. Different cells have been used in nerve repair, such as Schwann cell [15] and bone mesenchymal stem cells [16]. However, the clinical application of these cells is limited because they are difficult to obtain and proliferate slowly in culture [17]. Recently, adipose-derived stem cells (ADSCs) have attracted people’s attention as promising multipotent cells for application in various medical fields, such as wound healing [18–20], plastic surgery [21,22], and hair regrowth [23]. ADSCs delivered to an injured site may contribute to regeneration by secreting cytokines and growth factors [24], or by immunomodulatory effects [25, 26]. Especially, many studies have demonstrated the positive roles of

Peer review under responsibility of KeAi Communications Co., Ltd.

* Corresponding author.

** Corresponding author. Institute of Orthopedics, Chinese PLA General Hospital, Beijing Key Lab of Regenerative Medicine in Orthopedics, Key Lab of Musculoskeletal Trauma & War Injuries, PLA, No.28 Fuxing Road, Beijing, 100853, PR China.

E-mail addresses: zhengyudong@mater.ustb.edu.cn (Y. Zheng), pengjiang301@126.com (J. Peng).

¹ These authors contributed equally to this work and should be considered as co-first authors.

<https://doi.org/10.1016/j.bioactmat.2021.03.029>

Received 15 December 2020; Received in revised form 8 March 2021; Accepted 12 March 2021

2452-199X/© 2021 The Authors. Publishing services by Elsevier B.V. on behalf of KeAi Communications Co. Ltd. This is an open access article under the CC

BY-NC-ND license (<http://creativecommons.org/licenses/by-nc-nd/4.0/>).

ADSCs in nerve regeneration [13,27,28]. The advantages of ADSCs are that they have abundant sources, can be harvested by less-invasive procedures like liposuction, proliferate fast in culture, and can integrate in host tissues with immunological tolerance [29–31]. Therefore, ADSCs are regarded as an ideal cell source for transplantation in peripheral nerve regeneration [32].

As for the transplantation procedures, several methods have been adopted, such as (1) directly injecting cell suspension into NGCs [33, 34], (2) injecting cell suspension into NGCs followed by in vitro culture [35,36], and (3) mixing cells with Matrigel [14,29] or collagen [27,32] and then injecting them into NGCs. However, each of these methods has its own problems, such as cell leaking, low surviving rate due to lack of substrate during transplantation [37], complicated loading procedures, causing congestion of the NGCs, and risk of immunological reaction. Therefore, an efficient and convenient method for cell transplantation that is also compatible with existing commercial NGCs remains to be developed.

Microcarriers have been widely used in cell culture and delivery [38, 39]. Microcarriers are microspheres that are in favor of cell adhesion. With small size and large specific surface area, a small amount of microcarriers can provide a remarkably large surface area for cell loading [40]. More importantly, microcarriers can prevent cell anoikis during transplantation by providing substrates for cell adhesion, thus effectively improving cell survival [41]. Therefore, microcarriers have been used for cell transplantation in various medical fields, such as bone or osteochondral tissue engineering [42,43], muscle repair [44] and liver therapy [45]. Microcarrier-based cell transplantation has been applied in the treatment of central nervous system diseases. For example, in treating Parkinson's disease, microcarriers contribute to long-term functions by improving cell survival after implantation [46, 47]. For peripheral nerve regeneration, microcarriers have been used to deliver neurotrophic factors, such as glial cell line-derived neurotrophic factor (GDNF) [48,49] and nerve growth factor (NGF) [50]. The loading of neural cells on microcarriers have also been demonstrated in vitro [51,52]. However, to our knowledge, no study has been carried out as regards using microcarriers for cell transplantation in peripheral nerve repair.

Here, we fabricated novel macroporous, polylysine-decorated chitosan microcarriers (pl-CSMCs) for cell transplantation in nerve repair. We first prepared macroporous chitosan microcarriers (CSMCs) by the emulsion-phase separation method, and then decorated the CSMCs with polylysine to improve their cell affinity. Chitosan was chosen as the matrix material because it has good biocompatibility, biodegradability, plasticity, and is widely used as scaffold materials. Polylysine is a naturally occurring, biodegradable polypeptide with good biocompatibility [53]. Polylysine has been widely used to increase cell adhesion [54–56]. More importantly, polylysine has no immunogenicity. Therefore, we used polylysine to further increase the cell affinity of the CSMCs. The pl-CSMCs were then loaded with ADSCs using a simple centrifugation-based method. Finally, the ADSCs-laden pl-CSMCs were injected in electrospun polycaprolactone/chitosan (PCL/CS) NGCs to repair rat sciatic nerve defects. The effects of the cell-laden pl-CSMCs for nerve regeneration were systematically studied by gait analysis, histological evaluation, electrophysiology tests and gastrocnemius recovery evaluation.

2. Materials and methods

2.1. Materials

Chitosan (CAS:9012-76-4, >400 mPa s), glacial acetic acid (Cas:64-19-7, MW 60.05, ≥99.9%), paraffin liquid (CAS: 8042-47-5, 99%) and ethyl alcohol (CAS:64-17-5, MW 46.07, 99.7%) were purchased from Shanghai Macklin Biochemical Co., Ltd. Span-80 (CAS:1338-43-8, MW 428.6) and petroleum ether (CAS:8032-32-4, 60–90 °C) were purchased from Sinopharm Chemical Reagent Co., Ltd. ϵ -Polylysine (purified by

dialysis, MW 3.5–5 kDa) was obtained from Nanjing Shineking Biotechnology Co., Ltd.

2.2. Preparation of the CSMCs

The CSMCs were prepared by the emulsion-phase separation method. First, chitosan powder was dissolved in 2% acetic acid to get 2 wt% chitosan solution, which served as the aqueous phase. Span-80 was dropped in paraffin liquid and the mixture was stirred to be homogeneous, serving as the oil phase. The concentration of Span-80 was 1.8 wt %. The aqueous phase was added into the oil phase and stirred vigorously for 30 min to get the emulsion. The volume ratio of the aqueous phase to the oil phase was 1:2.5. The obtained emulsion was immediately poured into liquid nitrogen for quenching. Then the paraffin liquid in the emulsion was washed away with petroleum ether (precooled to $-20\text{ }^{\circ}\text{C}$), after which the microcarrier ice crystals were obtained. The ice crystals were then filtered out with a filter sieve and stored at $-20\text{ }^{\circ}\text{C}$ for 12 h. Then the ice crystals were freeze-dried in a freeze-dryer for 24 h to get the CSMCs. The CSMCs were washed with ethyl alcohol three times to get rid of the remaining oil phase, followed by washing with deionized water for another 3 times. The CSMCs were filtered out again and stored at $-20\text{ }^{\circ}\text{C}$ for 12 h. Finally, the CSMCs were freeze-dried for further use.

2.3. Decorating polylysine on the CSMCs

Polylysine was decorated on the CSMCs by hydrogen bonded self-assembly. Briefly, CSMCs were immersed in polylysine solution (5 g/L) and stored in refrigerator ($4\text{ }^{\circ}\text{C}$) for 12 h. Then the polylysine solution containing the CSMCs was stored at $-20\text{ }^{\circ}\text{C}$ for another 12 h. Finally, the pl-CSMCs were obtained by drying in a freeze dryer (LGJ-12, Beijing Songyuan).

2.4. Characterization of the pl-CSMCs

The microstructures were observed with a cold field emission scanning electron microscope (SU8020, Hitachi); the samples were coated with a layer of platinum to increase conductivity. The diameter and pore size of the pl-CSMCs were measured using the NIH ImageJ software. The FT-IR spectra of the microcarriers and polylysine were collected with an infrared spectrometer (SENSOR II, Bruker) by the pressed-disk technique. Briefly, 2 mg of the samples were mixed with 100 mg of potassium bromide, and grinded in an agate mortar until the mixture was uniform. Then potassium bromide tablets were prepared with a tablet press. Finally, the FT-IR spectra were collected with the infrared spectrometer in the range of $4000\text{--}400\text{ cm}^{-1}$ by the transmission mode.

2.5. Isolation and culture of ADSCs

In this study, animal experiments obtained written approval from the Ethics Committee of the Chinese PLA General Hospital, Beijing, China (approved number 2016-x9-07). ADSCs were isolated from 24 h-old SD rats by the method described elsewhere [30]. Briefly, the rats were sacrificed, and the inguinal adipose tissue was isolated, washed and cut into chyloform. Then the adipose tissue was digested with 1 mg mL^{-1} collagenase II (BS164, biosharp) diluted in DMEM/F-12 (11320082, ThermoFisher) at $37\text{ }^{\circ}\text{C}$ for 30 min. Next, the media was filtered with $70\text{-}\mu\text{m}$ filter screen and the digestion was stopped by adding equal amount of culture media. The media was centrifuged, and the supernatant discarded. Then PBS was added, and the centrifugation was repeated again. Finally, the harvested cells were cultured in cell incubator ($37\text{ }^{\circ}\text{C}$, 5% CO_2). Cells at passage 2–4 were used for subsequent experiments.

2.6. Cell viability on the pl-CSMCs

ADSCs were used to evaluate the cell viability on the pl-CSMCs; CSMCs serve as the control group. The microcarriers were sterilized by Co_{60} irradiation in Academy of Military Medical Sciences (Beijing, China). The irradiation dose was about 10–25 kGy; the samples were placed about 1 m away from the radiation source; the radiation time was 1000 min. The cultured cells were resuspended to a concentration of 5×10^4 cells mL^{-1} in DMEM/F-12. 10 mg of microcarriers were placed at the bottom of a 15-mL centrifuge tube, and then 2 mL of the cell suspension were added. The microcarriers were dispersed uniformly in the suspension by blowing with a pipette, after which the suspension was centrifuged at 1000 $r \min^{-1}$ for 3 min. The centrifuge tube was then placed in the incubator for 2 h to assure the adhesion of the cells on the microcarriers. Afterwards, the suspension containing the microcarriers were transferred to a cell culture plate and cultured in the incubator.

To determine the cell proliferation on the microcarriers, live-dead cell staining was carried out. After 1 and 3 days of incubation respectively, the cell medium in the culture plate was abandoned and the live cells were stained with live-dead cell staining kit (Abbkine) according to the specification. After staining, the cells on the microcarriers were observed under a fluorescence microscope (BX-50, Olympus). The quantity of the cells was semi-quantitatively determined according to the fluorescence intensity. After fluorescence observation, the cells on the microcarriers were fixed with 4% paraformaldehyde fix solution (Beyotime), dehydrated, and observed by SEM.

2.7. Loading ADSCs on the pl-CSMCs

The method for loading ADSCs on the pl-CSMCs was the same as described in the *Cell viability* section. To increase the loading efficiency, the cell density was raised to 2×10^5 mL^{-1} . The cells were cultured on the pl-CSMCs for 2 days before use. To examine the cells on the pl-CSMCs in a 3D view, the cells were stained with live-dead cell staining kit and observed with a confocal laser scanning microscope (FV1000, Olympus).

2.8. Animal surgery

30 female SD rats, weighing 200–220 g, were randomly divided into three groups: hollow, microcarrier and autograft. PCL/chitosan nerve conduits (12 mm long with inner diameter of 1.5 mm; the preparation methods were described elsewhere [57]) were used to repair the nerve defects in the hollow and microcarrier groups. The conduits were sterilized by Co_{60} irradiation before use. Prior to surgery, the rats were anaesthetized by intraperitoneal injection of sodium pentobarbital (3%, 30 $mg \text{ kg}^{-1}$). The right lower limb was sterilized with iodophor and a 20 mm incision was made. The sciatic nerve was isolated and a 10-mm segment the sciatic nerve was removed. For the microcarrier group, the distal nerve stump was first sutured 1 mm into the nerve conduit with 9-0 nylon monofilament suture. 50 μL of cell culture medium containing the ADSCs-laden pl-CSMCs (approximately 50 μg of pl-CSMCs by dry weight) was injected into the nerve conduit with a syringe. Then the proximal stump was sutured 1 mm into the conduit. The skin wound was sealed with 4-0 nylon suture. For the hollow group, 50 μL of pure cell culture medium without pl-CSMCs or cell was injected into the conduit, while the other steps were the same as the microcarrier group. For the autograft group, 10 mm of the sciatic nerve was cut off, reversed, and sutured back to the nerve stumps. After surgery, the rats were fed under standardized laboratory environment with day/night cycle.

2.9. Gait analysis

At 4, 8 and 12 weeks postoperatively, gait analysis was carried out to evaluate motor function recovery. The experiments were carried out

with a CatWalk footprint system (XT 10.6, Noldus). The rats were placed on a glass-bottomed walkway, and the gaits were recorded by a camera below. The data were processed with the CatWalk XT 10.6 software. The footprints were identified and measured manually. The sciatic functional index (SFI) and the stand/swing time ratio (SSR) were calculated by the software. Five rats in each group were evaluated.

2.10. Electrophysiological evaluation

At 12 weeks postoperatively, electrophysiologic testing was carried out to evaluate the function of nerve conduction. The rats were anaesthetized by intraperitoneal injection of sodium pentobarbital (3%, 30 $mg \text{ kg}^{-1}$). The right lower limb was sterilized and prepared for incision. The sciatic nerve and gastrocnemius muscle were exposed, and the compound muscle action potentials (CMAPs) were measured with an electromyogram recorder (Keypoint, Medtronic). Five rats in each group were tested.

2.11. Histological evaluation

After the electrophysiology tests, the rats were sacrificed by overdose of sodium pentobarbital. The whole nerve conduits were harvested and fixed in Zamboni-Stefanini solution (4 °C) for 24 h. For hematoxylin-eosin (HE) staining, the samples were embedded in optimal cutting temperature (OCT) compound (Tissue-Tek 4583, Sakura). The mid-portion of the samples were cut into transverse sections (7 μm thick) with an ultramicrotome (EM UC7, Leica). The sections were stained with HE staining kit (Solarbio) and observed under a microscope (BX51, Olympus). For toluidine blue (TB) staining, the nerve conduits were cut into 1 μm transverse sections and stained with TB solution (GP1052, Servicebio). Five fields for each group were randomly picked. The number of myelinated nerve fibers was counted with the NIH ImageJ software. For TEM observation, the midportion of the samples were cut into ultrathin sections (70 nm thick) and placed on copper slot grids with carbon support films. The sections were stained with lead citrate and uranyl acetate, and observed with a transmission electron microscope (HT7700, Hitachi). Ten fields for each group were randomly picked. The diameter of myelinated nerve fibers and thickness of the myelin sheath were measured with the NIH ImageJ software.

2.12. Gastrocnemius wet weight and histological evaluation

After the sacrifice of the rats, the gastrocnemius muscles on both sides of the rats were harvested. The wet weights of the gastrocnemius muscles were measured by an electronic scale; five rats in each group were measured. After that the gastrocnemius muscles were fixed in 4% formaldehyde for 2 h. For histological evaluation, the muscles were embedded in paraffin and cut into transverse sections (10 μm). After deparaffinization, the muscle sections were stained with Masson's trichrome stain Kit (Solarbio). The muscle tissue images were captured under a microscope and ten random fields were selected for each group. The muscle fiber diameters were measured with the NIH ImageJ software.

2.13. Statistics

Quantitative data were expressed as mean \pm standard deviation (SD). Statistical analysis was performed with the SPSS software (version 25.0, IBM). The data were compared using one-way analysis of variance (ANOVA), combined with Tukey's post hoc test. $P < 0.05$ are considered as statistically significant.

3. Results

3.1. The preparation process of the ADSCs-laden pl-CSMCs and their application in nerve repair

The preparation process of the ADSCs-laden pl-CSMCs and their application in peripheral nerve repair are illustrated in Fig. 1. First, macroporous CSMCs are prepared with chitosan by the emulsion-phase separation method. The macroporous structure increases the specific surface area and facilitates the loading of a large number of cells. To further increase the loading efficiency, the CSMCs are coated with polylysine, which has been widely used to increase cell adhesion. By immersing the CSMCs in polylysine solution and the following freeze-drying process, polylysine self-assembles on the surface of the CSMCs. The driving force for the self-assembly is the hydrogen-bond interaction between the amino groups in polylysine and the amino and hydroxyl groups in chitosan. Then ADSCs are loaded onto the pl-CSMCs by a sample centrifugation-based method. PCL/CS NGCs are prepared by electrospinning. During surgery, the ADSCs-laden pl-CSMCs are injected into the PCL/CS NGCs to repair rat sciatic nerve defects.

3.2. Characterization of the pl-CSMCs

The prepared microcarriers were first observed by SEM. As shown in Fig. 2a and b, the CSMCs have a spherical shape and a macroporous structure. The porosity of the CSMCs was measured to be $(85.4 \pm 2.6) \%$. After decoration of polylysine, the obtained pl-CSMCs reserve the spherical and porous morphology of the CSMCs (Fig. 2c). Further enlarged SEM image shows that there is crumb-like stuff on the surface of pl-CSMCs (Fig. 2d), which may be aggregated polylysine. The presence of polylysine is further confirmed by FT-IR spectra (Fig. 2e). As shown in Fig. 2e, for the spectrum of CSMCs, the broad absorption band at $3600\text{--}3100\text{ cm}^{-1}$ is attributed to O–H and N–H stretching vibrations; the two peaks at 2922 and 2860 cm^{-1} are ascribed to anti-symmetric and symmetric C–H stretching vibrations, respectively; the peak at 1647 cm^{-1} is due to the stretching vibrations of C=O in the remaining acetyl groups; the peak at 1565 cm^{-1} is attributed to N–H deformation vibrations; finally, the two peaks at 1152 and 1082 cm^{-1} are ascribed to the anti-symmetric stretching vibrations of C–O–C and stretching vibrations of C–O, respectively; these absorption peaks of CS correspond well with literature [58,59]. For the spectrum of polylysine, there are

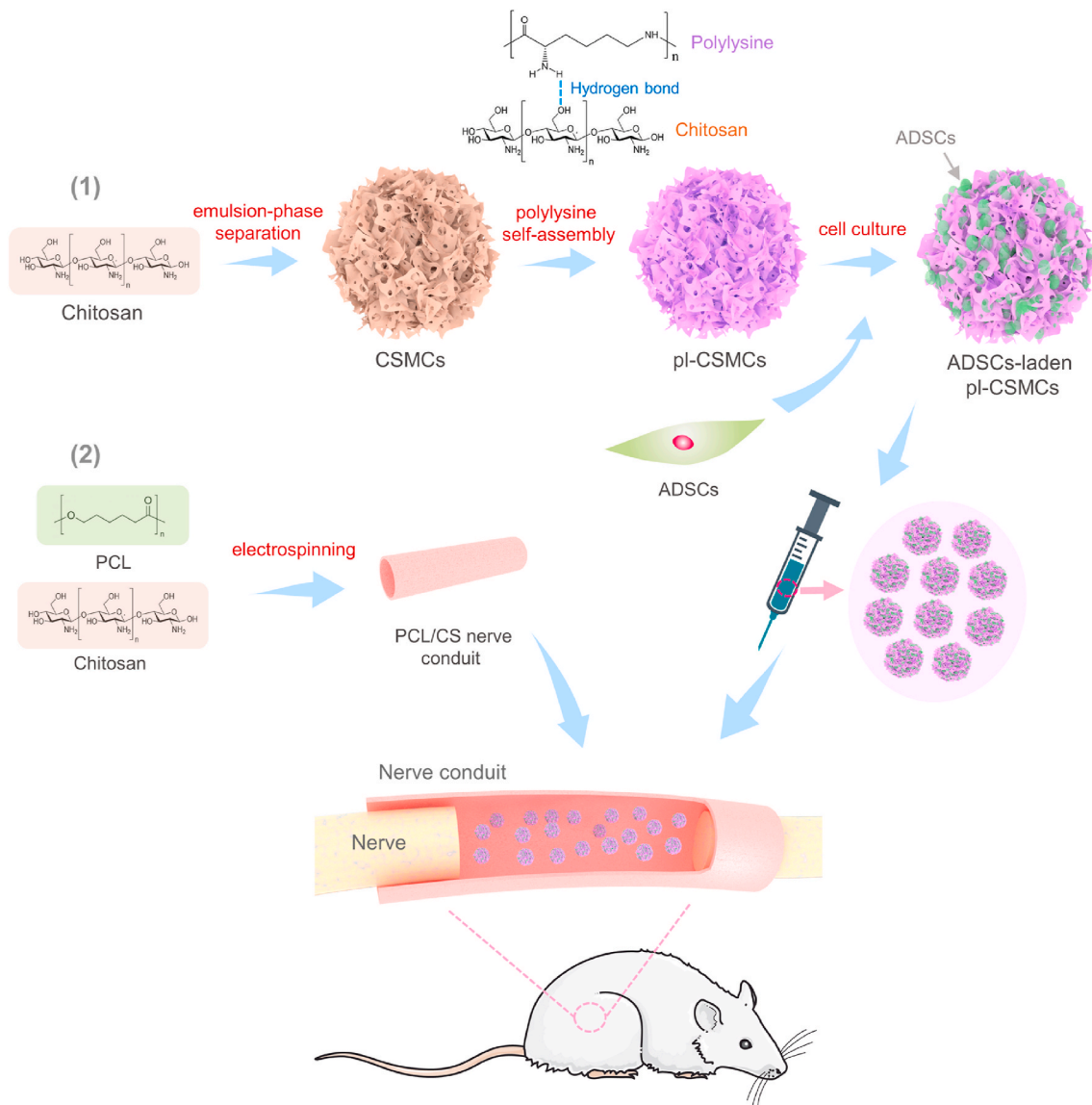


Fig. 1. Schematic of the preparation process of the ADSCs-laden pl-CSMCs and their application in nerve repair. Macroporous CSMCs are prepared with chitosan and decorated with polylysine to improve cell affinity; ADSCs are loaded onto the pl-CSMCs; the ADSCs-laden pl-CSMCs are injected into electrospun PCL/CS NGCs for nerve repair.

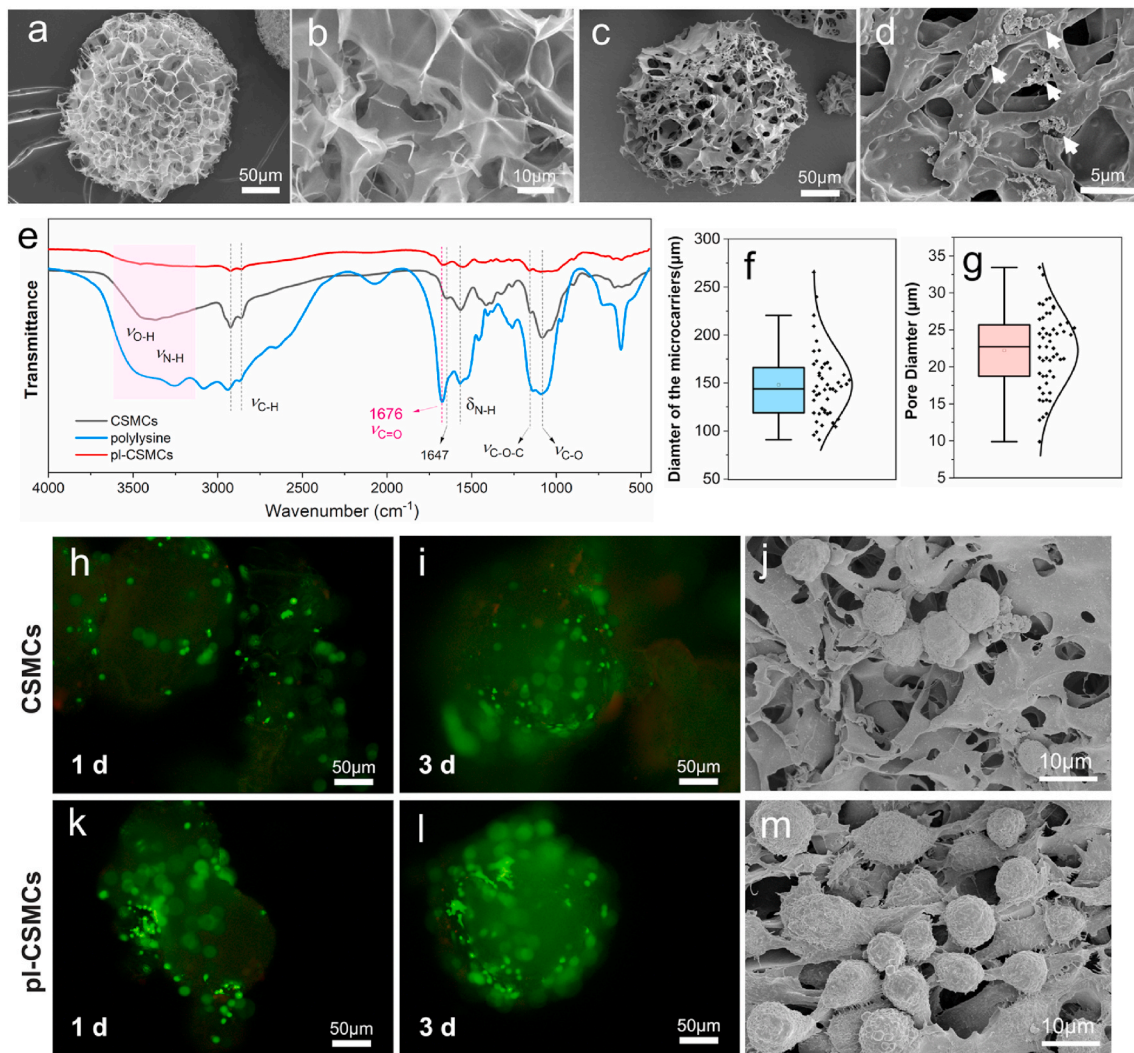


Fig. 2. Characterization of the pl-CSMCs and their cell affinity. (a, b) SEM images of the CSMCs; (c, d) SEM images of the pl-CSMCs; (e) FT-IR spectra of CSMCs, polylysine and pl-CSMCs; (f) Average diameter of the CSMCs; (g) Average pore diameter of the CSMCs; (h, i) Live cell staining of ADSCs grown on the CSMCs for 1 and 3 days; (k, l) Live cell staining of ADSCs grown on the pl-CSMCs for 1 and 3 days; (j, m) SEM images of ADSCs grown on the CSMCs and pl-CSMCs.

also absorption band or peaks for O–H, N–H and C–H stretching vibrations, and N–H deformation vibrations. However, compared with that of CSMCs, these is a strong peak at 1676 cm⁻¹, which is ascribed to C=O (Amide I band) stretching vibrations [60,61]. The peak for C=O stretching vibrations in the spectrum of polylysine is different from that of CSMCs because they are in different chemical environment. The spectrum of pl-CSMCs is basically the same with that of CSMCs. However, the absorption at 1676 cm⁻¹ is strengthened, which is in accordance with the Amide I band in polylysine. These facts prove the presence of polylysine in the pl-CSMCs. The average diameter of the pl-CSMCs is 148 ± 37 μm (Fig. 2f). This makes them injectable with common injection syringes. The small size of the pl-CSMCs can also avoid blockage of NGCs. The average pore diameter is 22 ± 5 μm (Fig. 2g), which is suitable for cell loading. The macroporous structure greatly increases the specific surface area, facilitating the loading of a large number of cells.

The cell affinity of the pl-CSMCs were studied by ADSC culture. As shown in Fig. 2h and k, after 1 day's culture, the cell densities on the CSMCs and pl-CSMCs are relatively low, but more cells are observed on the pl-CSMCs. After 3 days, more cells are observed on both CSMCs and pl-CSMCs (Fig. 2i and l), and the cell density on the pl-CSMCs is also higher than that of the CSMCs, as indicated by the fluorescence intensity. The cell adhesion on the MCs were also studied by SEM.

Compared with CSMCs, the cells on the pl-CSMCs presented a more spread form (Fig. 2j and m). These confirm the positive role of polylysine in increasing cell affinity.

3.3. pl-CSMCs-aided ADSC transplantation in nerve repair

To increase the cell loading efficiency in nerve repair, the initial cell density when culturing cells on the microcarriers was raised to 2 × 10⁵ mL⁻¹, from 5 × 10⁴ mL⁻¹ in the cell viability tests. The cells grown on the microcarriers were observed with a confocal laser scanning microscope. As shown in Fig. 3a–d (supplementary video), ADSCs are densely and uniformly packed on the pl-CSMCs, forming “cell balls”. The high cell loading density can be attributed to the three-dimensional, macroporous structure and the high cell affinity of polylysine. These further confirm that the pl-CSMCs can serve as good vehicles for cell transplantation. In rat sciatic nerve repair, the ADSCs-laden pl-CSMCs were injected into the PCL/CS NGCs with an injection syringe (Fig. 3e and f). The hollow group (pure cell culture medium without pl-CSMCs or cells was injected into the NGCs) and the autograft group serve as the control groups.

Supplementary video related to this article can be found at <https://doi.org/10.1016/j.bioactmat.2021.03.029>.

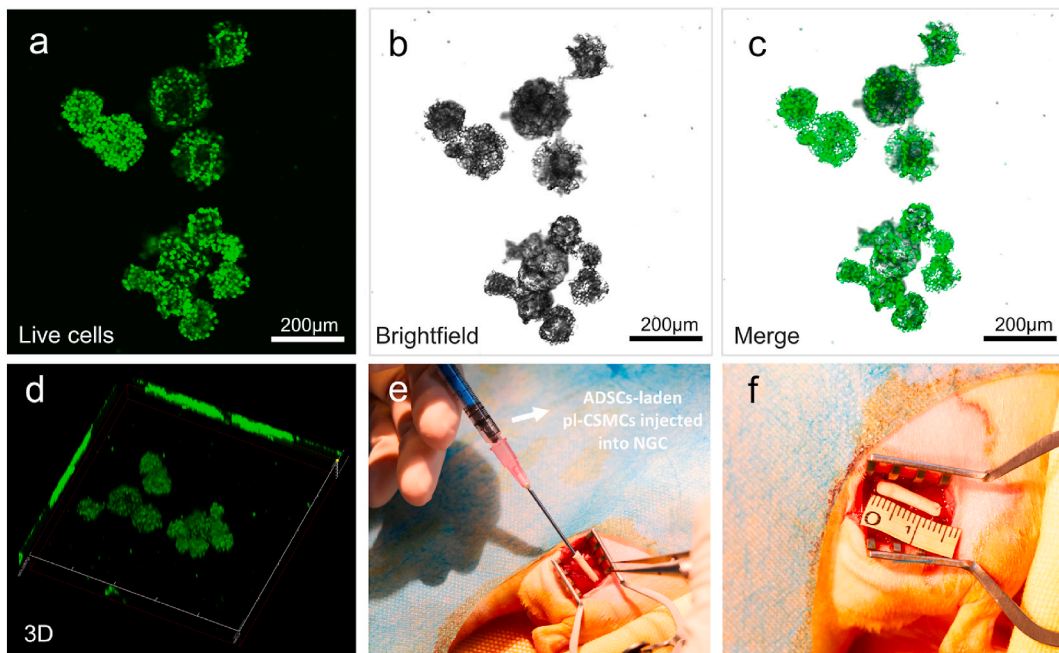


Fig. 3. pl-CSMCs-aided ADSC transplantation in nerve repair. (a–c) Confocal images of live ADSCs on the pl-CSMCs; (d) 3D view of the ADSCs-laden pl-CSMCs; (e, f) Injecting the ADSCs-laden pl-CSMCs into NGCs for rat sciatic nerve repair.

3.4. Histological evaluation of the regenerated nerves

12 weeks after surgery, the rats were sacrificed, and the regenerated nerves were harvested and observed first by HE staining. Fig. 4a–c shows the images of the implanted and harvested (insets) NGCs and nerve

autograft; no obvious tissue adhesion around the NGCs was observed. HE staining images show that the nerve tissue is scarce in the hollow group, while the nerve tissue is obviously denser in the microcarrier group, resembling that of the autograft (Fig. 4d–f). The HE images also show that there are more blood vessels in the microcarrier group than in

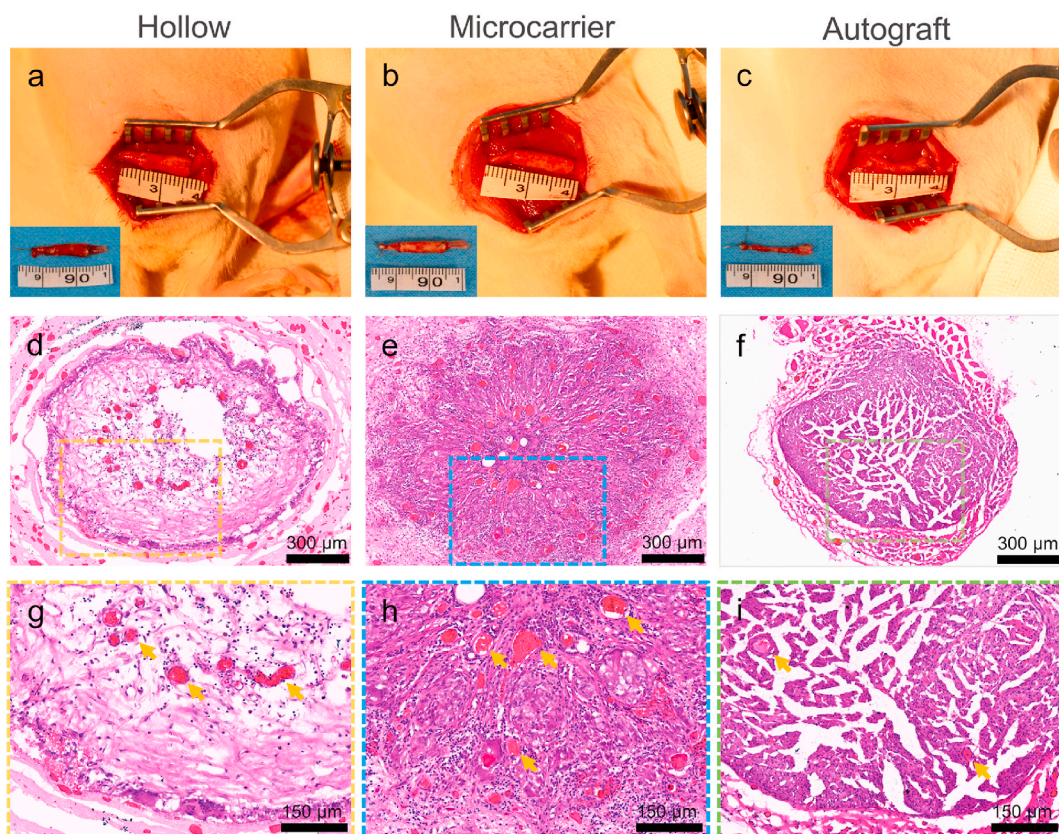


Fig. 4. Histological evaluation of the regenerated nerves. (a–c) NGCs and nerve autograft 12 weeks after implantation (insets: harvested NGCs and nerve autograft); (d–i) HE staining images of transverse sections of the regenerated nerve tissue at the midportion of the NGCs or autograft (yellow arrows indicate blood vessels).

the hollow group (Fig. 4g–i), which is also a sign of better recovery.

The regenerated nerves were further observed by TB staining and TEM. The TB staining images show that the density of regenerated myelinated nerve fibers is significantly higher in the microcarrier group than that in the hollow group (Fig. 5a–c, g). There is no significant difference between the microcarrier and the autograft groups as regards nerve density, although the nerve fibers were more uniformly distributed in the autograft group. The myelinated nerve fiber diameter and myelin sheath thickness were calculated according to the TEM results (Fig. 5d–f). The average diameter of the myelinated nerve fibers of the microcarrier group is $4.96 \pm 0.66 \mu\text{m}$, which is significantly larger than that of the hollow group ($2.75 \pm 0.62 \mu\text{m}$), while not significantly different from that of the autograft group ($5.69 \pm 1.11 \mu\text{m}$) (Fig. 5h). The myelin sheath thickness of the microcarrier group is also significantly larger than that of the hollow group, but lower than that of the autograft group (Fig. 5i).

3.5. Motor function recovery

Gait analysis was carried out to evaluate motor function recovery of the rats. The SFI of each group 4, 8 and 12 weeks after surgery are shown in Fig. 6a (the footprint images after 12 weeks are shown in Fig. 6c). After 4 weeks, the hollow, microcarrier and autograft groups all showed poor performance, with SFI lower than -90 . After 8 weeks, the SFI of the microcarrier group is -77.4 ± 5.5 , which is significantly higher than the hollow group (-89.1 ± 4.8), but lower than the autograft group (-63.3 ± 3.8). After 12 weeks, the SFI of the hollow, microcarrier and autograft groups are -78.6 ± 4.7 , -61.7 ± 4.9 and -49.6 ± 3.5 , respectively. The SFI of the microcarrier group is more significantly higher than the hollow group, although still lower than the autograft group. The SSR is also

an indicator for motor function. Fig. 6d shows the stand/swing time curves of the three groups (only the results after 12 weeks are shown), and the SSR values were shown in Fig. 6b. The SSR of the microcarrier group began to be significantly higher than the hollow group after 8 weeks. After 12 weeks, the SSR of the microcarrier group is 76%, higher than that of hollow group (65%) and close to the autograft group (83%).

3.6. Electrophysiology

The nerve conduction function was evaluated by electrophysiologic tests 12 weeks after surgery. Representative CMAP curves of the hollow, microcarrier and autograft groups are shown in Fig. 7a–c, respectively. As can be seen, the peak potential of the hollow group is small, only 24% of the normal side (Fig. 7d), indicating poor nerve conduction. Comparatively, the peak potential of the microcarrier group is 53% of the normal side, while that of the autograft group is 78%. The CAMP latency ratio of the microcarrier group is 1.52 ± 0.18 , which is significantly lower than that of the hollow group (2.20 ± 0.34), and not significantly different from that of the autograft group (1.35 ± 0.11) (Fig. 7e).

3.7. Gastrocnemius recovery

After the electrophysiologic tests, the gastrocnemius muscles on both sides were separated, weighed, and compared. Gross images show that the muscles of surgery side in the hollow group undergo severe atrophy (Fig. 8a). Comparatively, the surgery side muscles in the microcarrier group show much less atrophy, while those in the autograft group show comparable size with the normal side (Fig. 8b and c). The weight ratio of the microcarrier group ($\sim 45\%$) was significantly higher than that of the hollow group ($\sim 18\%$), but lower than the autograft group ($\sim 69\%$)

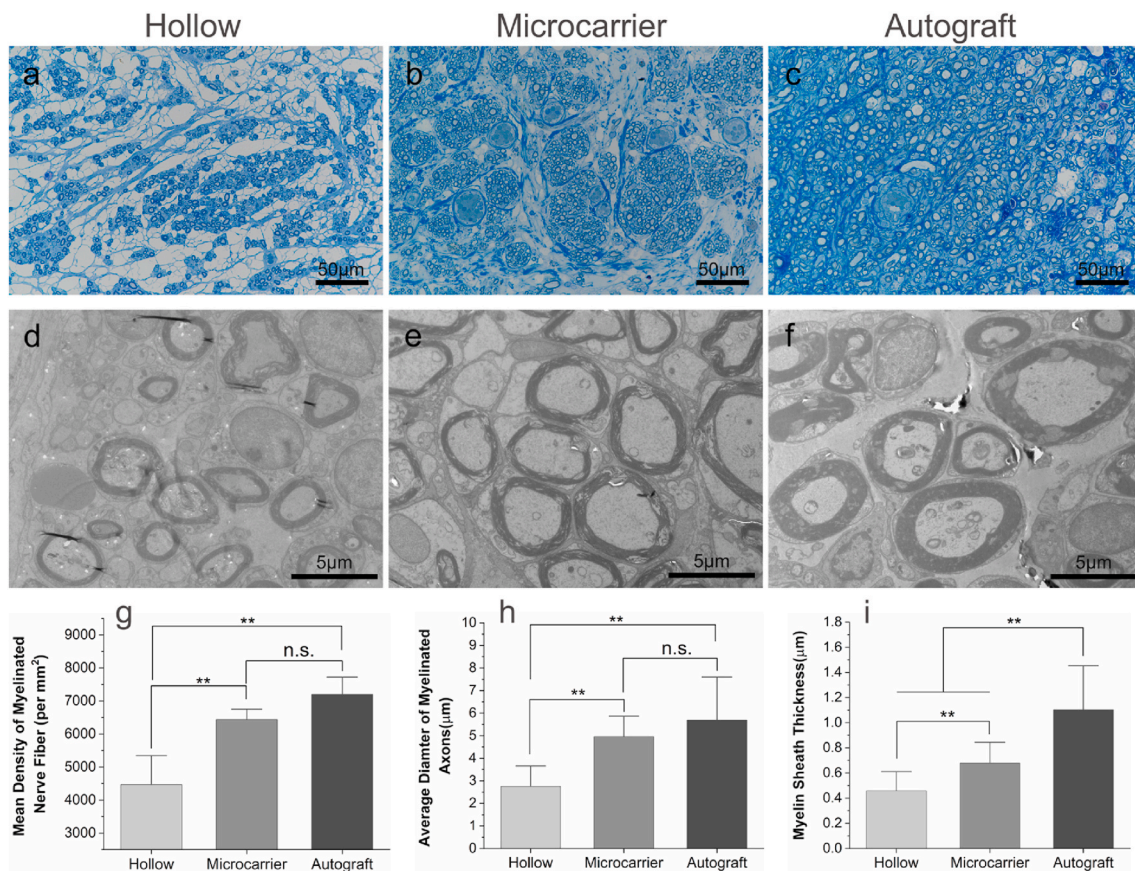


Fig. 5. Evaluation of the regenerated nerves by TB staining and TEM. (a–c) TB staining images of the transverse sections of the regenerated nerve tissue at the midportion of the NGCs or autograft; (d–f) The corresponding TEM images; (g) Mean density of myelinated nerve fiber ($n = 5$); (h) Average diameter of the myelinated axons ($n = 10$); (i) Myelin sheath thickness ($n = 10$). ** $p < 0.01$; n.s.: no significance.

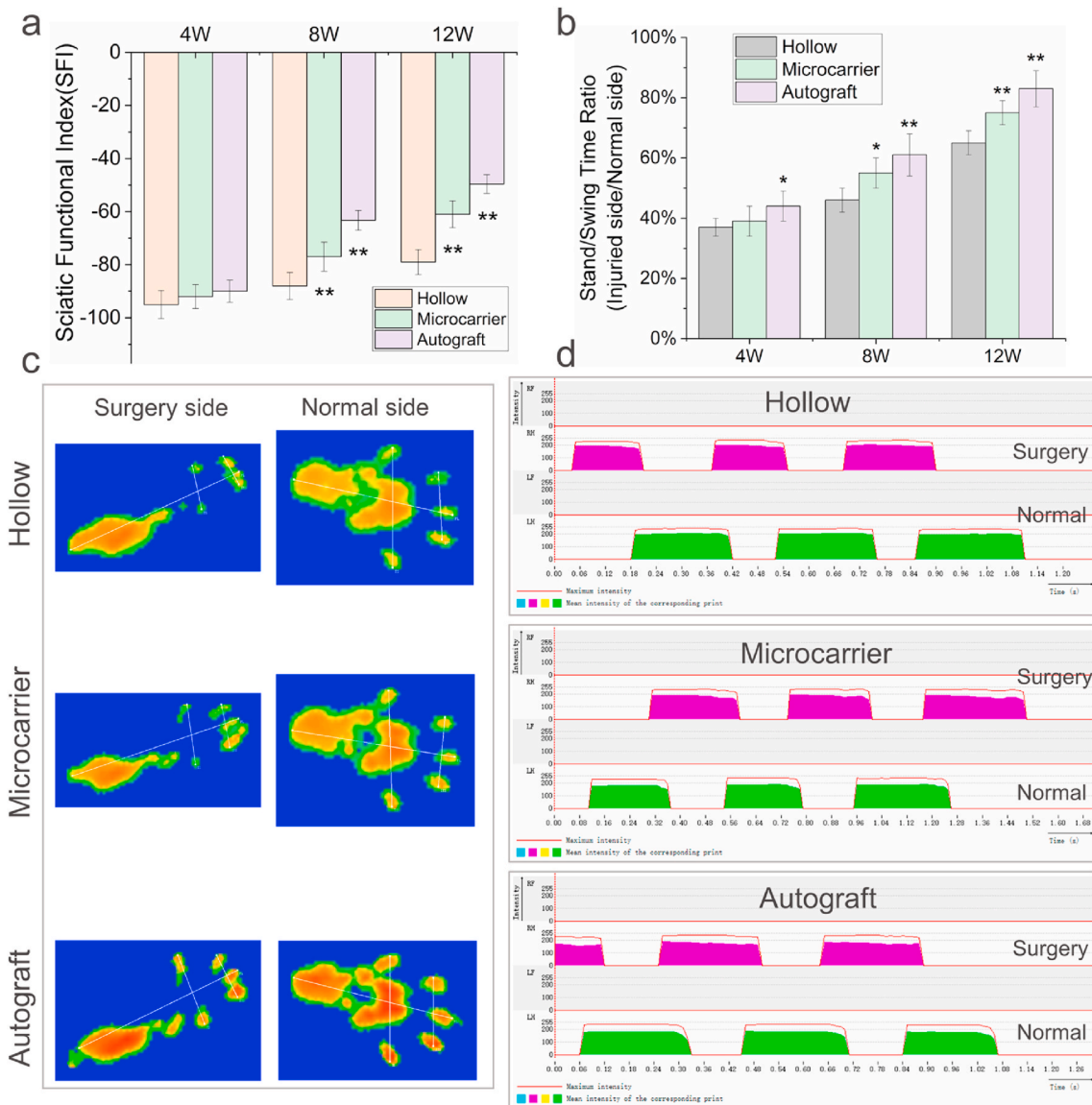


Fig. 6. Gait analysis. (a) SFI values of the hollow, microcarrier and autograft groups 4, 8 and 12 weeks after surgery; (b) Corresponding SSR of the three groups; (c) Representative footprint images of the hollow, microcarrier and autograft groups 12 weeks after surgery; (d) Representative stand/swing time curves of the three groups 12 weeks after surgery. n = 5 for each group; *p < 0.05, **p < 0.01.

(Fig. 8g). Masson’s trichrome staining images (Fig. 8d–f) show that the hollow group has obvious hyperplasia of collagen fibers, while the microcarrier group shows much less. The mean cross-sectional area of the muscle fibers in the hollow, microcarrier and autograft group are 162 ± 30 , 843 ± 373 and $1227 \pm 253 \mu\text{m}^2$, respectively (Fig. 8h). The muscle fibers of the microcarrier group are much thicker than the those of the hollow group.

4. Discussion

In this study, we investigated whether transplanting ADSCs into NGCs with microcarriers could be an effective strategy to improve nerve regeneration. We prepared polylysine-decorated, macroporous CSMCs and loaded them with ADSCs for rat sciatic nerve repair. Our results show that the pl-CSMCs can serve as efficient cell culture and transplantation vehicles, and that adding the ADSCs-laden pl-CSMCs into NGCs can effectively improve the outcomes of nerve regeneration, as demonstrated by histological and functional evaluation.

Nerve regeneration is a complicated process that requires various

guidance cues and the synergistic regulation of multiple cytokines [62]. Sample use of one or two growth factors, such as NGF or brain-derived neurotrophic factor (BDNF), can hardly mimic the naturally occurred processes. Besides, the growth factors are prone to be inactivated, and the release profile is hard to control. On the other hand, transplanted cells can release a series of regeneration-related cytokines in a sustained and controlled manner, creating a microenvironment suitable for regeneration [11,30,63]. Therefore, compared with the delivery of neurotrophic factors, cell transplantation may be a more promising strategy to promote nerve regeneration.

ADSCs, with easy access and abundant sources, show great promise in nerve regeneration. Further, ADSCs can be differentiated into Schwann cell-like cells and express higher levels of neurotrophic factors such as NGF and BDNF [27,34]. Both undifferentiated and differentiated ADSCs have been used in nerve regeneration. The advantages of differentiated ADSCs are that they can participate more actively in the regeneration process and promote better recovery [64]. However, the time-consuming differentiation process may lead to delayed treatment. Comparatively, undifferentiated ADSCs are more readily accessible with

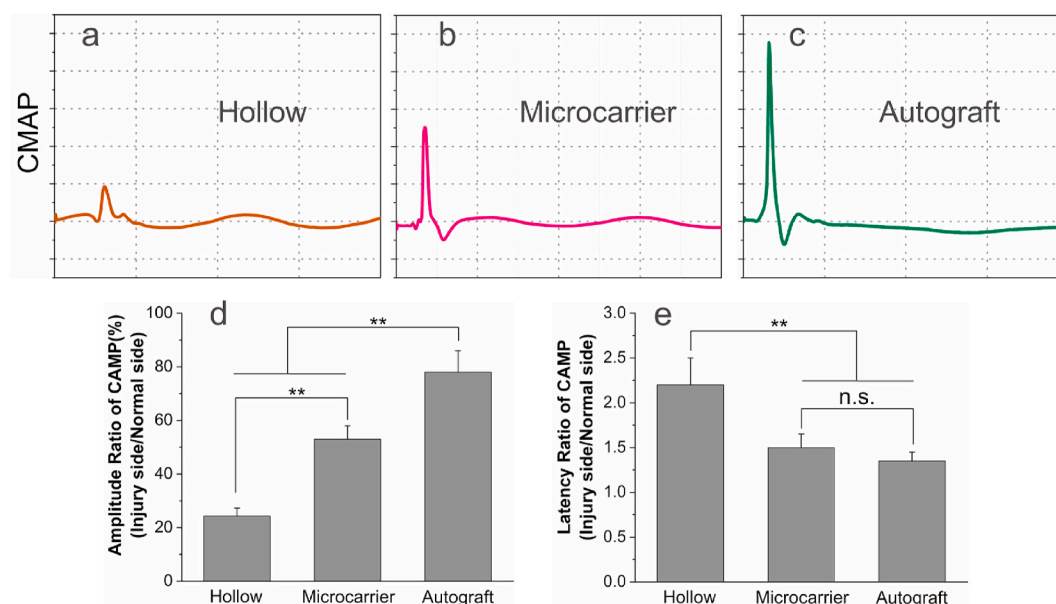


Fig. 7. Electrophysiological test results 12 weeks after surgery. (a–c) Representative CMAP curves of the hollow, microcarrier and autograft groups; (d) Peak amplitude ratio of CMAP (injury side/normal side) of the three groups; (e) The latency ratio of CMAP (injury side/normal side) of the three groups. $n = 5$ for each group; ** $p < 0.01$.

a liposuction process, resulting in timelier treatment. Although there are concerns that undifferentiated ADSCs may undergo unwanted differentiation in vivo, the risk is low [17]. In this study, we try to investigate the feasibility of microcarrier-based cell transplantation in nerve repair. Therefore, we chose undifferentiated ADSCs for convenience. Nevertheless, differentiated ADSCs can still be used in this process. Further, in the future, the differentiation of the ADSCs and be directly carried out on the pl-CSMCs, leading to rapid expansion of cells, and saving an extra loading process.

We first prepared macroporous, polylysine-decorated chitosan microcarriers. Chitosan has been widely used for preparing microspheres [65,66]. The good plasticity of chitosan allows for fine tuning of the microstructure. To facilitate cell loading and injection, the diameter, porosity, and pore size of the microcarriers had been carefully tuned by controlling the parameters in the preparation process, such as the concentrations of the liquid and oil phase, the volume ratio of the oil phase to the aqueous phase, and the stirring rate. After extensive trials, macroporous microcarriers with suitable pore size for cell loading and suitable diameter for injection were prepared. Polylysine effectively improved the cell affinity of the CSMCs and hence the loading efficiency (Fig. 2h–m). Polylysine is a hydrophilic, positively charged amino acid polymer. The cell affinity of polylysine might be originated from its hydrophilicity and the electrostatic interaction between its positively charged amino groups and the negatively charged ions on cell membrane [53]. Compared with other adhesion promoting materials such as collagen and gelatin, polylysine has even lower immunogenicity and relatively higher safety. In this study, we initially used two polylysine solutions, with polylysine concentrations of 2 g/L and 5 g/L, respectively, to treat the CSMCs. We found that the CSMCs treated with 5 g/L of polylysine had better cell affinity. For convenience, we used pl-CSMCs prepared with 5 g/L of polylysine in our following experiments.

We loaded ADSCs on the pl-CSMCs using a simple centrifugation-based method. Compared with the rotating bioreactor-based method [67], our method is simple, convenient, and not instrument-dependent. ADSCs can grow uniformly on the pl-CSMCs with high density, indicating that the pl-CSMCs are good 3D cell culture scaffolds (Fig. 3a–d). The ADSCs-laden pl-CSMCs can be conveniently injected into NGCs with an injection syringe (Fig. 3e). This makes it easy to apply them in clinical practice. Compared with other methods, such as directly injecting cell

suspension into NGCs, injecting cell suspension into NGCs followed by in vitro culture, and mixing cells with Matrigel or collagen, our method holds several advantages. First, the 3D and porous structure of the microcarriers facilitates the cultivation of a large number of cells in vitro. Second, thanks to the large surface area of the microcarriers, a large number of cells can be transferred using a relatively small number of materials, thus avoiding congestion of the NGCs. Thirdly, the microcarriers can provide substrate for cell to adhere during transplantation, which can effectively prevent cell anoikis and thus improve cell survival.

We used multiple indicators to evaluate the effects of the ADSCs-laden pl-CSMCs in nerve regeneration. The TB staining results indicate that the ADSCs-laden pl-CSMCs improved the density of the regenerated nerves (Fig. 5a–c, g). Nerve remyelination is a sign of mature regeneration, and larger diameter of myelinated axon and thicker myelin sheath are related to better nerve conduction. The TEM results show that nerve myelination was effectively improved by adding the ADSC-laden pl-CSMCs (Fig. 5d–f, h and i). The gait results indicate that the ADSC-laden pl-CSMCs effectively improved motor function recovery (Fig. 6). The amplitude of CMAP reflects the number of reinnervated muscle fibers, and the latency of CMAP reflects the degree of myelination [29]. Our electrophysiological results suggest that the ADSCs-laden pl-CSMCs promoted nerve reinnervation (Fig. 7). The results also indicate improved nerve myelination, which is consistent with the TEM results. Finally, the gastrocnemius recovery results also suggest that the ADSCs-laden pl-CSMCs contributed to nerve reinnervation and decreased muscle atrophy (Fig. 8). In conclusion, these results jointly suggest that loading the ADSCs-laden pl-CSMCs into NGCs effectively improved nerve regeneration.

The exact role of ADSCs in nerve regeneration remains vague. Some studies have concluded that ADSCs contribute to regeneration by trophic effects rather than in vivo differentiation [68]. Apart from this, ADSCs may also function by their immunomodulatory effects [26]. Our results further confirmed the positive effects of ADSCs in nerve regeneration, although the results were still not as good as the autograft group. This is probably due to the complexity of nerve regeneration. The transplantation of cells is beneficial but not enough. Multiple components should be added in order to imitate the features of natural nerve.

While we believe our results show the promising future of the ADSCs-

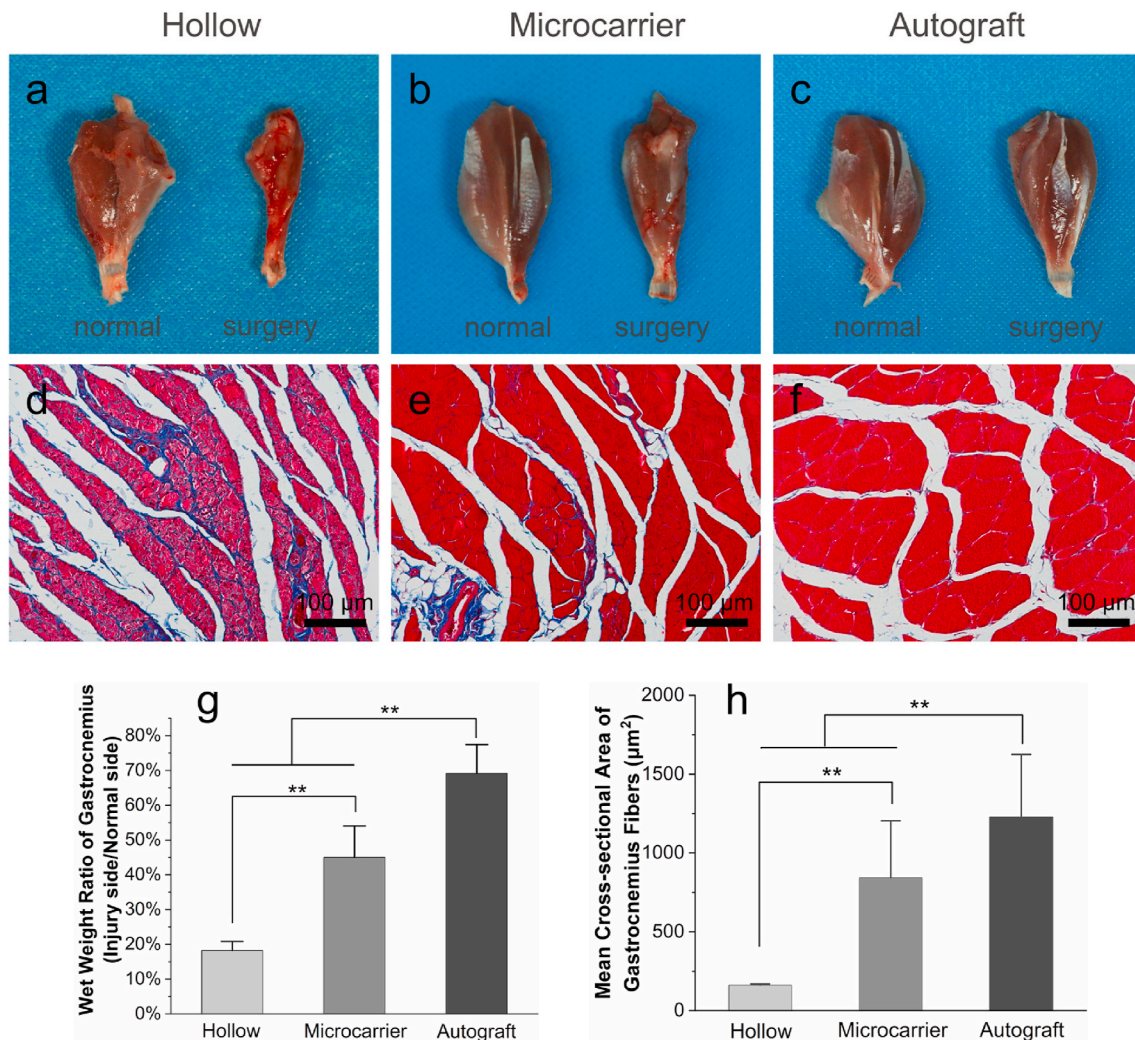


Fig. 8. Gastrocnemius muscle evaluation 12 weeks after surgery. (a–c) Gross images of the harvested gastrocnemius muscles; (d–f) Masson's trichrome staining images of cross-sections of the gastrocnemius muscles (the blue-stained areas indicate hyperplasia of collagen fibers); (g) Wet weight ratio of the gastrocnemius muscles; (e) Mean cross-sectional area of the gastrocnemius muscles. $n = 5$ for each group; ** $p < 0.01$.

laden pl-CSMCs in peripheral nerve repair, there are some limitations in our study. First, we did not compare the effects of our microcarrier-based cell transplantation method with other methods. The advantages of our method lie not only in the cell delivery process, but also in cell culture. In the cell delivery process, our method excludes a trypsin digestion procedure, which can avoid damage to the cells, while the microcarriers can also provide substrate for adhesion, avoiding cell anoikis and further improving cell survival [46,47]. In the cell culture process, our microcarrier-based method has the advantage of rapid cell expansion. It is known that, for peripheral nerve injury, good functional recovery depends on timely repair. Microcarriers are excellent tools for rapid cell expansion. For autologous cell therapy, microcarriers can help to rapidly expand the patient's own ADSCs; while for allogeneic cell therapy, off-the-shelf ADSCs-laden microcarriers can be directly used for more timely nerve repair. In this study, we have demonstrated the feasibility of microcarrier-based cell delivery. With advantages in both the cell culture and delivery processes, we believe that our ADSCs-laden pl-CSMCs are promising in peripheral nerve repair.

Secondly, the effects of the different dosage of the ADSCs-laden pl-CSMCs to nerve regeneration were not investigated. Different dosage of the pl-CSMCs results in different amount of the ADSCs transplanted. Optimization of the dosage of the ADSCs-laden pl-CSMCs may help us obtain better outcomes. Thirdly, the living situation of the ADSCs after *in vivo* transplantation was not investigated. The improved regeneration

in the microcarrier group indicates the positive role of the transplanted ADSCs. However, the activities of the ADSCs in the NGCs are not clear. More efforts need to be done to reveal the activities of the ADSCs *in vivo*.

5. Conclusions

In summary, in this work, we demonstrated for the first time microcarrier-based ADSC transplantation in peripheral nerve repair. We prepared novel, macroporous pl-CSMCs for efficient transplantation of ADSCs. The pl-CSMCs have an average diameter of $148 \pm 37 \mu\text{m}$ and an average pore diameter of $22 \pm 5 \mu\text{m}$, which are suitable for cell loading and application in NGCs. The pl-CSMCs also have good cytocompatibility, with ADSCs growing densely-packed on the pl-CSMCs, forming 3D "cell balls". The ADSCs-laden pl-CSMCs can be conveniently injected into NGCs with an injection syringe. The ADSCs-laden pl-CSMCs loaded into NGCs effectively improved nerve regeneration in a rat sciatic nerve defect model, in terms of axon growth, nerve myelination, nerve reinnervation, and motor function recovery. Our work demonstrates a new strategy to transplant ADSCs into NGCs for cell therapy. It is worth noting that this strategy is compatible with the NGCs available in market. With efficient cell transplantation and convenient operation, the ADSCs-laden pl-CSMCs hold good potential in peripheral nerve repair.

CRedit authorship contribution statement

Yi Sun: Conceptualization, Investigation, Methodology, Writing – original draft. **Xiaoqi Chi:** Conceptualization, Investigation, Methodology. **Haoye Meng:** Investigation, Resources. **Mengjiao Ma:** Investigation. **Jing Wang:** Investigation. **Zhaoxuan Feng:** Methodology. **Qi Quan:** Methodology. **Yansen Wang:** Writing – review & editing. **Yajie Xie:** Methodology. **Yudong Zheng:** Resources, Supervision, Validation, Funding acquisition, Writing – review & editing. **Jiang Peng:** Resources, Supervision, Validation, Funding acquisition.

Declaration of competing interest

The authors declare that they have no known competing financial interests or personal relationships that could have appeared to influence the work reported in this paper.

Acknowledgements

This work is supported by National Natural Science Foundation of China (Grant No. 51773018, 51973018) and Key Research and Development Projects of People's Liberation Army (BWS17J036).

Appendix A. Supplementary data

Supplementary data to this article can be found online at <https://doi.org/10.1016/j.bioactmat.2021.03.029>.

References

- M.D. Sarker, S. Naghieh, A.D. McInnes, D.J. Schreyer, X.b. Chen, Regeneration of peripheral nerves by nerve guidance conduits: influence of design, biopolymers, cells, growth factors, and physical stimuli, *Prog. Neurobiol.* 171 (2018) 125–150.
- A.C. Pinho, A.C. Fonseca, A.C. Serra, J.D. Santos, J.F.J. Coelho, Peripheral nerve regeneration: current status and new strategies using polymeric materials, *Adv. Healthc. Mater.* 5 (21) (2016) 2732–2744.
- P.A. Wieringa, A.R.G. de Pinho, S. Micera, R.J.A. van Wezel, L. Moroni, Biomimetic architectures for peripheral nerve repair: a review of biofabrication strategies, *Adv. Healthc. Mater.* 7 (8) (2018).
- S. Yi, L. Xu, X.S. Gu, Scaffolds for peripheral nerve repair and reconstruction, *Exp. Neurol.* 319 (2019).
- Z.-F. Zhou, F. Zhang, J.-G. Wang, Q.-C. Chen, W.-Z. Yang, N. He, Y.-Y. Jiang, F. Chen, J.-J. Liu, Electrospinning of PELA/PPY fibrous conduits: promoting peripheral nerve regeneration in rats by self-originated electrical stimulation, *ACS Biomater. Sci. Eng.* 2 (9) (2016) 1572–1581.
- L. Huang, L. Zhu, X. Shi, B. Xia, Z. Liu, S. Zhu, Y. Yang, T. Ma, P. Cheng, K. Luo, J. Huang, Z. Luo, A compound scaffold with uniform longitudinally oriented guidance cues and a porous sheath promotes peripheral nerve regeneration in vivo, *Acta Biomater.* 68 (2018) 223–236.
- S. Tang, J. Zhu, Y. Xu, A.P. Xiang, M.H. Jiang, D. Quan, The effects of gradients of nerve growth factor immobilized PCLA scaffolds on neurite outgrowth in vitro and peripheral nerve regeneration in rats, *Biomaterials* 34 (29) (2013) 7086–7096.
- Q. Quan, H. Meng, B. Chang, L. Hong, R. Li, G. Liu, X. Cheng, H. Tang, P. Liu, Y. Sun, J. Peng, Q. Zhao, Y. Wang, S. Lu, Novel 3-D helix-flexible nerve guide conduits repair nerve defects, *Biomaterials* 207 (2019) 49–60.
- W. Zhu, K.R. Tringale, S.A. Woller, S. You, S. Johnson, H. Shen, J. Schimelman, M. Whitney, J. Steinauer, W. Xu, T.L. Yaksh, Q.T. Nguyen, S. Chen, Rapid continuous 3D printing of customizable peripheral nerve guidance conduits, *Mater. Today* 21 (9) (2018) 951–959.
- Y. Sun, Q. Quan, H.y. Meng, Y.d. Zheng, J. Peng, Y.x. Hu, Z.x. Feng, X. Sang, K. Qiao, W. He, X.q. Chi, L. Zhao, Enhanced neurite outgrowth on a multiblock conductive nerve scaffold with self-powered electrical stimulation, *Adv. Healthc. Mater.* 8 (10) (2019) 1900127.
- M. Farina, J.F. Alexander, U. Thekkedath, M. Ferrari, A. Grattoni, Cell encapsulation: overcoming barriers in cell transplantation in diabetes and beyond, *Adv. Drug Deliv. Rev.* 139 (2019) 92–115.
- P. Assinck, G.J. Duncan, B.J. Hilton, J.R. Plemler, W. Tetzlaff, Cell transplantation therapy for spinal cord injury, *Nat. Neurosci.* 20 (5) (2017) 637–647.
- Y.-Y. Hsueh, Y.-J. Chang, T.-C. Huang, S.-C. Fan, D.-H. Wang, J.-J. Chen, C.-C. Wu, S.-C. Lin, Functional recoveries of sciatic nerve regeneration by combining chitosan-coated conduit and neurosphere cells induced from adipose-derived stem cells, *Biomaterials* 35 (7) (2014) 2234–2244.
- Q. Ao, C.-K. Fung, A.Y.-P. Tsui, S. Cai, H.-C. Zuo, Y.-S. Chan, D.K.-Y. Shum, The regeneration of transected sciatic nerves of adult rats using chitosan nerve conduits seeded with bone marrow stromal cell-derived Schwann cells, *Biomaterials* 32 (3) (2011) 787–796.
- Y. Qian, X. Zhao, Q. Han, W. Chen, H. Li, W. Yuan, An integrated multi-layer 3D-fabrication of PDA/RGD coated graphene loaded PCL nanoscaffold for peripheral nerve restoration, *Nat. Commun.* 9 (2018).
- A. Ladak, J. Olson, E.E. Tredget, T. Gordon, Differentiation of mesenchymal stem cells to support peripheral nerve regeneration in a rat model, *Exp. Neurol.* 228 (2) (2011) 242–252.
- R. Zhang, J.M. Rosen, The role of undifferentiated adipose-derived stem cells in peripheral nerve repair, *Neural Regen. Res.* 13 (5) (2018) 757–763.
- H. Mizuno, M. Tobita, A.C. Uysal, Concise review: adipose-derived stem cells as a novel tool for future regenerative medicine, *Stem Cell.* 30 (5) (2012) 804–810.
- G. Eke, N. Mangir, N. Hasirci, S. MacNeil, V. Hasirci, Development of a UV crosslinked biodegradable hydrogel containing adipose derived stem cells to promote vascularization for skin wounds and tissue engineering, *Biomaterials* 129 (2017) 188–198.
- N.C. Cheng, W.J. Lin, T.Y. Ling, T.H. Young, Sustained release of adipose-derived stem cells by thermosensitive chitosan/gelatin hydrogel for therapeutic angiogenesis, *Acta Biomater.* 51 (2017) 258–267.
- P. Gentile, M.G. Scioli, A. Bielli, A. Orlandi, V. Cervelli, Concise review: the use of adipose-derived stromal vascular fraction cells and platelet rich plasma in regenerative plastic surgery, *Stem Cell.* 35 (1) (2017) 117–134.
- P. Gentile, A. Kothari, D. Casella, C. Calabrese, Fat graft enhanced with adipose-derived stem cells in aesthetic breast augmentation: clinical, histological, and instrumental evaluation, *Aesthetic Surg. J.* 40 (9) (2020) 962–977.
- P. Gentile, S. Garcovich, Advances in regenerative stem cell therapy in androgenic alopecia and hair loss: Wnt pathway, growth-factor, and mesenchymal stem cell signaling impact analysis on cell growth and hair follicle development, *Cells* 8 (5) (2019).
- J.M. Gimble, A.J. Katz, B.A. Bunnell, Adipose-derived stem cells for regenerative medicine, *Circ. Res.* 100 (9) (2007) 1249–1260.
- E. Gonzalez-Rey, M.A. Gonzalez, N. Varela, F. O'Valle, P. Hernandez-Cortes, L. Rico, D. Buescher, M. Delgado, Human adipose-derived mesenchymal stem cells reduce inflammatory and T cell responses and induce regulatory T cells in vitro in rheumatoid arthritis, *Ann. Rheum. Dis.* 69 (1) (2010) 241–248.
- N. Puissant, C. Barreau, P. Bourin, C. Clavel, J. Corre, C. Bousquet, C. Taureau, B. Cousin, M. Abbal, P. Laharrague, L. Penicaud, L. Casteilla, A. Blancher, Immunomodulatory effect of human adipose tissue-derived adult stem cells: comparison with bone marrow mesenchymal stem cells, *Br. J. Haematol.* 129 (1) (2005) 118–129.
- M. Georgiou, J.P. Golding, A.J. Loughlin, P.J. Kingham, J.B. Phillips, Engineered neural tissue with aligned, differentiated adipose-derived stem cells promotes peripheral nerve regeneration across a critical sized defect in rat sciatic nerve, *Biomaterials* 37 (2015) 242–251.
- M.-N. Hsu, H.-T. Liao, K.-C. Li, H.-H. Chen, T.-C. Yen, P. Makarevich, Y. Parfyonova, Y.-C. Hu, Adipose-derived stem cell sheets functionalized by hybrid baculovirus for prolonged GDNF expression and improved nerve regeneration, *Biomaterials* 140 (2017) 189–200.
- F. Sun, K. Zhou, W.-j. Mi, J.-h. Qiu, Combined use of decellularized allogeneic artery conduits with autologous transdifferentiated adipose-derived stem cells for facial nerve regeneration in rats, *Biomaterials* 32 (32) (2011) 8118–8128.
- X. Sun, Y. Zhu, H.y. Yin, Z.y. Guo, F. Xu, B. Xiao, W.L. Jiang, W.m. Guo, H.y. Meng, S.b. Lu, Y. Wang, J. Peng, Differentiation of adipose-derived stem cells into Schwann cell-like cells through intermittent induction: potential advantage of cellular transient memory function, *Stem Cell Res. Ther.* 9 (2018) 133.
- L. Bacakova, J. Zarubova, M. Travnickova, J. Musilkova, J. Pajorova, P. Slepicka, N.S. Kasalkova, V. Svoricik, Z. Kolska, H. Motarjemi, M. Molitor, Stem cells: their source, potency and use in regenerative therapies with focus on adipose-derived stem cells - a review, *Biotechnol. Adv.* 36 (4) (2018) 1111–1126.
- Y. Zhang, H. Luo, Z. Zhang, Y. Lu, X. Huang, L. Yang, J. Xu, W. Yang, X. Fan, B. Du, P. Gao, G. Hu, Y. Jin, A nerve graft constructed with xenogeneic acellular nerve matrix and autologous adipose-derived mesenchymal stem cells, *Biomaterials* 31 (20) (2010) 5312–5324.
- S. Walsh, J. Biernaskie, S.W.P. Kemp, R. Midha, Supplementation OF acellular nerve grafts with SKIN derived precursor cells promotes peripheral nerve regeneration, *Neuroscience* 164 (3) (2009) 1097–1107.
- P.G. di Summa, P.J. Kingham, W. Raffoul, M. Wiberg, G. Terenghi, D. F. Kalbermatten, Adipose-derived stem cells enhance peripheral nerve regeneration, *J. Plast. Reconstr. Aesthetic Surg.* 63 (9) (2010) 1544–1552.
- Y. Wei, K. Gong, Z. Zheng, A. Wang, Q. Ao, Y. Gong, X. Zhang, Chitosan/silk fibroin-based tissue-engineered graft seeded with adipose-derived stem cells enhances nerve regeneration in a rat model, *J. Mater. Sci. Mater. Med.* 22 (8) (2011) 1947–1964.
- J. Hu, Q.-T. Zhu, X.-L. Liu, Y.-b. Xu, J.-K. Zhu, Repair of extended peripheral nerve lesions in rhesus monkeys using acellular allogeneic nerve grafts implanted with autologous mesenchymal stem cells, *Exp. Neurol.* 204 (2) (2007) 658–666.
- D. Jgamadze, J. Bergen, D. Stone, J.-H. Jang, D.V. Schaffer, E.Y. Isacoff, S. Pautot, Colloids as mobile substrates for the implantation and integration of differentiated neurons into the mammalian brain, *PLoS One* 7 (1) (2012).
- A.K.L. Chen, S. Reuveny, S.K.W. Oh, Application of human mesenchymal and pluripotent stem cell microcarrier cultures in cellular therapy: achievements and future direction, *Biotechnol. Adv.* 31 (7) (2013) 1032–1046.
- B.Y. Li, X. Wang, Y. Wang, W.L. Gou, X.L. Yuan, J. Peng, Q.Y. Guo, S.B. Lu, Past, present, and future of microcarrier-based tissue engineering, *J. Orthop. Transl.* 3 (2) (2015) 51–57.
- S.M. Naqvi, S. Vedicherla, J. Gansau, T. McIntyre, M. Doherty, C.T. Buckley, Living cell factories - electrosprayed microcapsules and microcarriers for minimally invasive delivery, *Adv. Mater.* 28 (27) (2016) 5662–5671.

- [41] B. Newland, P.B. Welzel, H. Newland, C. Renneberg, P. Kolar, M. Tsurkan, A. Rosser, U. Freudenberg, C. Werner, Tackling cell transplantation anoxia: an injectable, shape memory cryogel microcarrier platform material for stem cell and neuronal cell growth, *Small* 11 (38) (2015) 5047–5053.
- [42] R. Levato, J. Visser, J.A. Planell, E. Engel, J. Malda, M.A. Mateos-Timoneda, Biofabrication of tissue constructs by 3D bioprinting of cell-laden microcarriers, *Biofabrication* 6 (3) (2014).
- [43] R.A. Perez, A. El-Fiqi, J.H. Park, T.H. Kim, J.H. Kim, H.W. Kim, Therapeutic bioactive microcarriers: Co-delivery of growth factors and stem cells for bone tissue engineering, *Acta Biomater.* 10 (1) (2014) 520–530.
- [44] R. Ahmadi, N. Mordan, A. Forbes, R.M. Day, Enhanced attachment, growth and migration of smooth muscle cells on microcarriers produced using thermally induced phase separation, *Acta Biomater.* 7 (4) (2011) 1542–1549.
- [45] T.T. Lau, C. Wang, S.W. Png, K. Su, D.-A. Wang, Genipin-crosslinked microcarriers mediating hepatocellular aggregates formation and functionalities, *J. Biomed. Mater. Res.* 96A (1) (2011) 204–211.
- [46] G.J.R. Delcroix, E. Garbayo, L. Sindji, O. Thomas, C. Vanpouille-Box, P.C. Schiller, C.N. Montero-Menei, The therapeutic potential of human multipotent mesenchymal stromal cells combined with pharmacologically active microcarriers transplanted in hemi-parkinsonian rats, *Biomaterials* 32 (6) (2011) 1560–1573.
- [47] S. Saporta, C. Borlongan, J. Moore, E. Mejia-Millan, S.L. Jones, P. Bonness, T. S. Randall, R.C. Allen, T.B. Freeman, P.R. Sanberg, Microcarrier enhanced survival of human and rat fetal ventral mesencephalon cells implanted in the rat striatum, *Cell Transplant.* 6 (6) (1997) 579–584.
- [48] J.L. Roam, P.K. Nguyen, D.L. Elbert, Controlled release and gradient formation of human glial-cell derived neurotrophic factor from heparinated poly(ethylene glycol) microsphere-based scaffolds, *Biomaterials* 35 (24) (2014) 6473–6481.
- [49] L.E. Kokai, A.M. Ghaznavi, K.G. Marra, Incorporation of double-walled microspheres into polymer nerve guides for the sustained delivery of glial cell line-derived neurotrophic factor, *Biomaterials* 31 (8) (2010) 2313–2322.
- [50] W. Zeng, M. Rong, X. Hu, W. Xiao, F. Qi, J. Huang, Z. Luo, Incorporation of chitosan microspheres into collagen-chitosan scaffolds for the controlled release of nerve growth factor, *PLoS One* 9 (7) (2014).
- [51] D. Shendi, D.R. Albrecht, A. Jain, Anti-Fas conjugated hyaluronic acid microsphere gels for neural stem cell delivery, *J. Biomed. Mater. Res.* 105 (2) (2017) 608–618.
- [52] L. Yao, F. Phan, Y. Li, Collagen microsphere serving as a cell carrier supports oligodendrocyte progenitor cell growth and differentiation for neurite myelination in vitro, *Stem Cell Res. Ther.* 4 (2013).
- [53] S.C. Shukla, A. Singh, A.K. Pandey, A. Mishra, Review on production and medical applications of epsilon-polylysine, *Biochem. Eng. J.* 65 (2012) 70–81.
- [54] J.E. Collazos-Castro, J.L. Polo, G.R. Hernandez-Labrado, V. Padial-Canete, C. Garcia-Rama, Bioelectrochemical control of neural cell development on conducting polymers, *Biomaterials* 31 (35) (2010) 9244–9255.
- [55] S. Joo, K. Kang, Y. Nam, In vitro neurite guidance effects induced by polylysine pinstripe micropatterns with polylysine background, *J. Biomed. Mater. Res.* 103 (8) (2015) 2731–2739.
- [56] S.S. Rao, N. Han, J.O. Winter, Polylysine-modified PEG-based hydrogels to enhance the neuro-electrode interface, *J. Biomater. Sci. Polym. Ed.* 22 (4–6) (2011) 611–625.
- [57] Q. Quan, H.-Y. Meng, B. Chang, G.-B. Liu, X.-Q. Cheng, H. Tang, Y. Wang, J. Peng, Q. Zhao, S.-B. Lu, Aligned fibers enhance nerve guide conduits when bridging peripheral nerve defects focused on early repair stage, *Neural Regen. Res.* 14 (5) (2019) 903–912.
- [58] A. Zajac, J. Hanuza, M. Wandas, L. Dyminska, Determination of N-acetylation degree in chitosan using Raman spectroscopy, *Spectrochim. Acta Mol. Biomol. Spectrosc.* 134 (2015) 114–120.
- [59] J. Arata Badano, N. Vanden Braber, Y. Rossi, L. Diaz Vergara, L. Bohl, C. Porporatto, R. Dario Falcone, M. Montenegro, Physicochemical, in vitro antioxidant and cytotoxic properties of water-soluble chitosan-lactose derivatives, *Carbohydr. Polym.* 224 (2019).
- [60] T. Li, C. Wen, Y. Dong, D. Li, M. Liu, Z. Wang, S. Janaswamy, B. Zhu, S. Song, Effect of epsilon-polylysine addition on kappa-carrageenan gel properties: rheology, water mobility, thermal stability and microstructure, *Food Hydrocolloids* 95 (2019) 212–218.
- [61] T. Xu, B. Chi, M. Chu, Q. Zhang, S. Zhan, R. Shi, H. Xu, C. Mao, Hemocompatible epsilon-polylysine-heparin microparticles: a platform for detecting triglycerides in whole blood, *Biosens. Bioelectron.* 99 (2018) 571–577.
- [62] M.C. Dodla, M. Alvarado-Velez, V.J. Mukhatyar, R.V. Bellamkonda, *Peripheral Nerve Regeneration, Principles of Regenerative Medicine*, Elsevier, 2019, pp. 1223–1236.
- [63] A.J. Reid, M. Sun, M. Wiberg, S. Downes, G. Terenghi, P.J. Kingham, Nerve repair with adipose-derived stem cells protects dorsal root ganglia neurons from apoptosis, *Neuroscience* 199 (2011) 515–522.
- [64] A. Faroni, G. Terenghi, A.J. Reid, Adipose-derived stem cells and nerve regeneration: promises and pitfalls, in: S. Geuna, I. Perroteau, P. Tos, B. Battiston (Eds.), *Tissue Engineering of the Peripheral Nerve: Stem Cells and Regeneration Promoting Factors*, 2013, pp. 121–136.
- [65] J. Fang, Y. Zhang, S. Yan, Z. Liu, S. He, L. Cui, J. Yin, Poly(L-glutamic acid)/chitosan polyelectrolyte complex porous microspheres as cell microcarriers for cartilage regeneration, *Acta Biomater.* 10 (1) (2014) 276–288.
- [66] M. Pan, Z. Tang, J. Tu, Z. Wang, Q. Chen, R. Xiao, H. Liu, Porous chitosan microspheres containing zinc ion for enhanced thrombosis and hemostasis, *Mater. Sci. Eng. C-Mater. Biol. Appl.* 85 (2018) 27–36.
- [67] Y. Wang, X. Yuan, K. Yu, H. Meng, Y. Zheng, J. Peng, S. Lu, X. Liu, Fabrication of nanofibrous microcarriers mimicking extracellular matrix for functional microtissue formation and cartilage regeneration (vol 171, pg 118, 2018), *Biomaterials* 183 (2018) 171–172.
- [68] K.B. Carlson, P. Singh, M.M. Feaster, A. Ramnarain, C. Pavlides, Z.L. Chen, W. M. Yu, M.L. Feltri, S. Strickland, Mesenchymal stem cells facilitate axon sorting, myelination, and functional recovery in paralyzed mice deficient in schwann cell-derived laminin, *Glia* 59 (2) (2011) 267–277.